

Evaluation of the Variation in Dynamic Load Factor Throughout a Highly Skewed Steel I-Girder Bridge

Yousif Almoosi

Department of Civil Engineering
College of Engineering
University of Baghdad
Baghdad, Iraq
yousif@udel.edu

Jennifer McConnell

Department of Civil and Environmental Engineering
College of Engineering
University of Delaware
Delaware, USA
righman@udel.edu

Nazar Oukaili

Department of Civil Engineering
College of Engineering
University of Baghdad
Baghdad, Iraq
nazar.oukaili@coeng.uobaghdad.edu.iq

Abstract—The Dynamic Load Factor (DLF) is defined as the ratio between the maximum dynamic and static responses in terms of stress, strain, deflection, reaction, etc. DLF adopted by different design codes is based on parameters such as bridge span length, traffic load models, and bridge natural frequency. During the last decades, a lot of researches have been made to study the DLF of simply supported bridges due to vehicle loading. On the other hand, fewer works have been reported on continuous bridges especially with skew supports. This paper focuses on the investigation of the DLF for a highly skewed steel I-girder bridge, namely the US13 Bridge in Delaware State, USA. Field testing under various load passes of a weighed load vehicle was used to validate full-scale three-dimensional finite element models and to evaluate the dynamic response of the bridge more thoroughly. The results are presented as a function of the static and dynamic tensile and compressive stresses and are compared to DLF code provisions. The result shows that most codes of practice are conservative in the regions of the girder that would govern the flexural design. However, the DLF sometimes exceeds the code-recommended values in the vicinity of skewed supports. The discrepancy of the DLF determined based on the stress analysis of the present study, exceeds by 13% and 16% the values determined according to AASHTO (2002) for tension and compression stresses respectively, while, in comparison to BS5400, the differences reach 6% and 8% respectively.

Keywords—dynamic load factor; steel bridges; skewed bridges; codes of practice; field test; finite element analysis

I. INTRODUCTION

Skewed supports occur when the supporting abutments for the girders are not normal to the girder lines. This may be required due to the characteristics of the intersecting roadways or due to the geological terrain. Since skew angles increase the interaction between the steel girders and the cross-frames or

diaphragms, the behavior of bridges with skewed supports becomes more complicated than that in bridges with normal supports. Differential girder deflections, obtuse and acute angle corners, unbalanced construction loads, and the possibility for unequal girder lengths are among other characteristics of skew bridges that subject the girders to significant torsional and lateral moments induced by moving truck loads, which may affect the dynamic responses. More accurate knowledge of the dynamic responses will lead to safer and more economical designs of new bridges and to more effective evaluation of existing ones. DLF is defined as the ratio between the maximum dynamic and static responses [1]:

$$\text{Dynamic Load Allowance (DLA)} = \frac{D_{dyn} - D_{stat}}{D_{stat}} \quad (1)$$

$$\text{Dynamic Load Factor (DLF)} = 1 + \text{DLA} = \frac{D_{dyn}}{D_{stat}} \quad (2)$$

where D_{dyn} and D_{stat} are the dynamic and static responses of the bridge girders, respectively (e.g. deflections, strains, stress, or reactions). In the present study, the responses refer to the maximum tensile and compressive stresses respectively.

Today, design codes and specifications recommend the use of a dynamic load factor as a function of span length, natural frequency, and traffic load models, regardless of the type of bridge. Studies have also shown that DLF is influenced by parameters such as the road surface condition, vehicle weight, speed, the number of axles, and bridge materials and type. The American Association of State Highway and Transportation Officials (AASHTO (2002)) [2] specified the Dynamic Load Allowance (DLA) as a function of the bridge span length:

$$\text{DLA (IM)} = \frac{15.24}{L_{(\text{in meters})} + 38.10} \leq 30\% \quad (3a)$$

Corresponding author: Yousif Almoosi

$$DLA (IM) = \frac{50}{L_{(in\ feet)} + 125} \leq 30\% \quad (3b)$$

where L is the clear span length measured from center to center of the bearing supports. This empirical equation has been in effect since 1944. Similar to the expression given by AASHTO, the Japan Road Association also defines the DLA as a function of the bridge span length [3]. However, in the new AASHTO LRFD [4], for strength considerations, the DLA adopted is equal to 0.33 of the truck effects.

The 1983 Ontario Highway Bridge Design Code [5], and the 1992 Australia's Bridge Design Code [6], both specify the DLF as a function of the first longitudinal natural frequency of the bridge. The DLA values fall between 0.2 and 0.4, with the higher values corresponding to frequencies between 2.5 and 4.5Hz. In some codes such as the 2003 EUROCODE [7], and the 2006 BS5400-2 [8], two types of loading for highway bridges are considered, namely the HA and HB loading for normal and abnormal traffic loads respectively. For both loading types, a constant DLA of 0.25 is used. The review of the aforementioned codes also reveals what factors are not considered in DLF. These include different bridge types, skews, curvatures, and cross-section properties (except for how these variables may influence the natural frequency in the Ontario and Australian specifications) and the fact that a single DLF is used for the entire bridge versus various points in the bridge having different DLFs. There is a large volume of research data on impact factors and bridge-vehicle interaction. The most relevant ones to this study concern the verification of impact factor relations introduced in design codes, and comparison with empirical and numerical results. Authors in [9] implemented a study on the Dynamic Amplification Factor (DAF) by evaluating continuous beam bridges and conducting vehicle bridge interaction analysis. The result showed that when resonance condition was approached, the DAF increased, and therefore, vehicle speed influenced the DAF in the studied girder bridges.

Authors in [10], proposed a method to evaluate the impact factors for fatigue design purposes taking into account the effect of the deterioration of the road surface condition, vehicle velocity, and bridge span length of steel I-girder bridges. Maximum stress range instead of the maximum stress is used to calculate the conventional impact factor. The new impact factor can be used to correlate fatigue-induced damage. A non-linear dynamic simulation was conducted in [1] to determine the dynamic impact for composite steel bridges. The modeling involved rigid bodies (vehicles) connected to nonlinear suspensions. The composite steel girder bridge assembly consists of 3D thin-walled beam elements. The parametric study includes vehicle velocity, span length, elastomeric bearings stiffness, vehicle mass, and eccentricity with respect to deck centerline. The conclusion is that current code-specified values are adequate for normal design situations. Authors in [11] investigated the impact factor for concrete-steel composite I-girder bridges. FEA was conducted using ABAQUS for 120 different bridges, considering parameters such as span length, girders number, and the number of traffic lanes in order to model the traffic loads. The vehicle-bridge interaction was disregarded. The outcome of this research was

that the impact factor for composite bridges based on the AASHTO formula is over-estimated for moment and deflection and is under-estimated for support reaction. Authors in [12] evaluated the impact factor for simple and continuous beams subjected to moving vehicles. The parameters that were taken into account are the frequency ratio of vehicle-bridge interaction, bridge damping, and road pavement roughness. The study revealed that the impact factor outputs of the bridge responses (e.g. moment, support reactions, and deflections) are different and suggested new formulas for the impact factor. The DLFs according to different graphic codes can be seen graphically in [1].

Figure 1 shows the DLF of the bridge that is the subject of the present research compared to the DLFs determined according to the above-mentioned codes as well as the Italian, French, and West German ones. This shows that the span length for the bridge of interest results in the highest variability among the different codes.

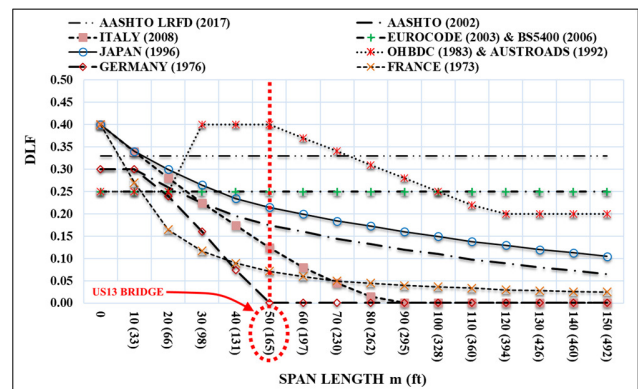


Fig. 1. Dynamic load factors for US13 Bridge according to different practice codes. Data taken from [1].

The current study aims to evaluate the DLF of a highly skewed steel I-girder bridge with perpendicular cross-frames and the variation in DLF along the length of a representative girder. This is accomplished using a bridge previously field-tested to validate a finite element analysis and then using the validated model to simulate various traffic loadings. A case study including a 3D FEA model for the same bridge specifications and dimensions but with staggered cross-frames configuration is implemented to investigate the effect of different arrangements of bracing systems on the bridge dynamic response and thus on DLFs values. This is an extension of the prior field test that suggested that the DLF was highly variable at a small number of points where it was possible to install field instrumentation. Thus, the presentation of results focuses on the computation of DLF at key points along the length of the girders.

II. BRIDGE FIELD TESTING

A. Bridge General Description

The bridge of interest, labeled as the US13 Bridge, is a 65° heavily skewed steel I-girder bridge in Delaware State, USA (Figure 2(a)).

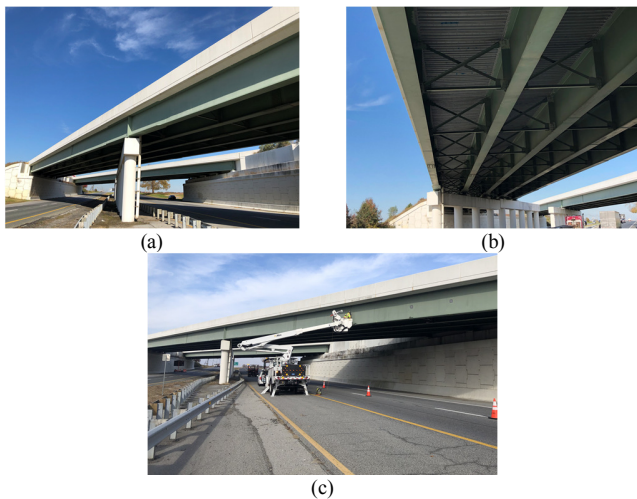


Fig. 2. US13 Bridge in Delaware State, USA, (a) general view, (b) perpendicular cross-frame configuration, (c) gauge installing and lane closing.

Twin spans carry the north- and south-bound lanes. The bridge consists of two continuous spans of equal lengths of 50m (165ft). There are 5 girders spaced 2.9m (9.5ft) on center with exterior girders spaced 0.86m (2.83ft) and 1.16m (3.83ft) away from the outer edge of the bridge concrete guard wall on the west and east sides respectively. Therefore, the total width of the bridge is 13.37m (44.67ft), carrying two 3.65m (12ft) lanes, a 3.65m (12ft) shoulder on the west side, and a 1.82m (6ft) shoulder on the east side. The concrete guard wall located on each side has a width of 0.4m (1.34ft) and a height of 0.86m (2.83ft). The bridge contains inline X-shaped cross-frames (between girders and at pier location) oriented perpendicular to the girders, as shown in Figure 3, which are connected to the girders using full-depth connection plates. Also, inline K-shaped cross-frames are used in the vicinity of the abutment supports.

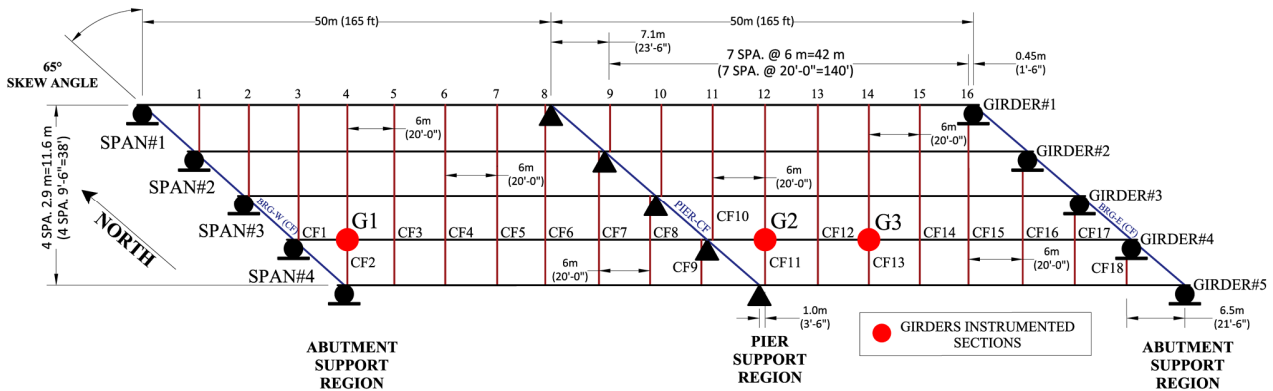


Fig. 3. Framing plan and instrumentation locations for US13 Bridge.

B. Instrumentation Layout and Loading Pattern

Bridge Diagnostics Inc. ST-350 strain gauges (BDI gauges) [13] and their associated data-acquisition system were used in the field test. Specifically, 12 strain gauges were installed on girder #4 at 3 different cross-sections labeled G1, G2, and G3 (Figure 3). Each of these cross-sections was instrumented with 4 strain gauges (Figure 4). One pair of them was placed 5cm (2in) away from the outer edges of the bottom surface of the bottom flange. These positions are labeled as BF-1 and BF-2. The other pair was placed on the opposite sides of the web at approximately mid-height of the web and are labeled W-1 and W-2. One additional pair was used only for the numerical FEA located at the bottom of the web and labeled as WB-1 and WB-2. Three different truck passes, with 24km/hr (15mph) speed, were conducted for the load test (Figure 5). Pass #1 had the loaded truck travel down the center of the left lane. This position was intended to maximize the stress and induce differential deflection in Girder #4. Pass #2 was designed to produce a high level of stress in both Girder #3 and Girder #4, while Pass #3 had the truck travel with the left side wheels aligned with the centerline of the two lanes, intending to

maximize differential deflections between the instrumented girder and the adjacent one [14]. Three additional passes are implemented using FEA and are labeled as Passes #4–#6 which mimic Passes #1–#3 respectively, but with different travel speed of 104km/hr (65mph).

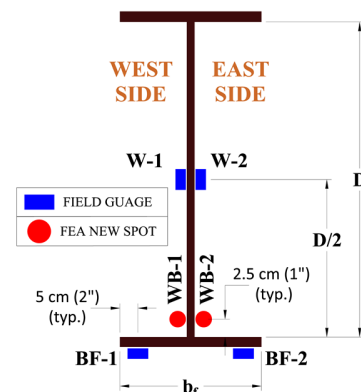


Fig. 4. Instrumentation locations across the cross-section of the US13 Bridge during the field test and FEA.

III. FINITE ELEMENT ANALYSIS

A. Geometry, Meshing, Elements, Materials, and Boundary Conditions

The geometry of the bridge for both static and dynamic FEA models was created according to the structural plans provided by the bridge owner (the Delaware Department of

Transportation). Software like AutoCAD-3D, FEMAP, NX Nastran, and ABAQUS/CAE were used to perform the bridge final finite element model [15] (Figure 6). Over one million four-node reduced-integration shell elements [16], were used for modeling all girders, cross-frames, and stay-in-place profiled metal deck forms in each of the static and dynamic models.

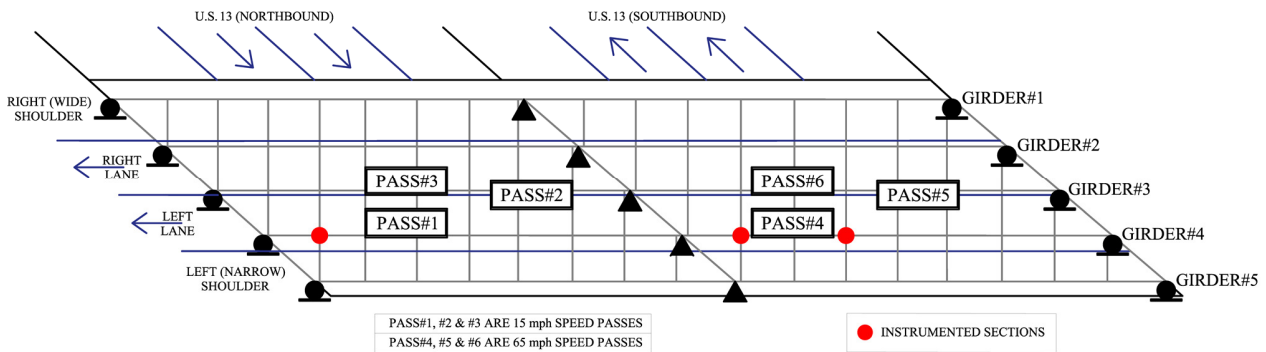


Fig. 5. Truck load passes on the US13 Bridge.

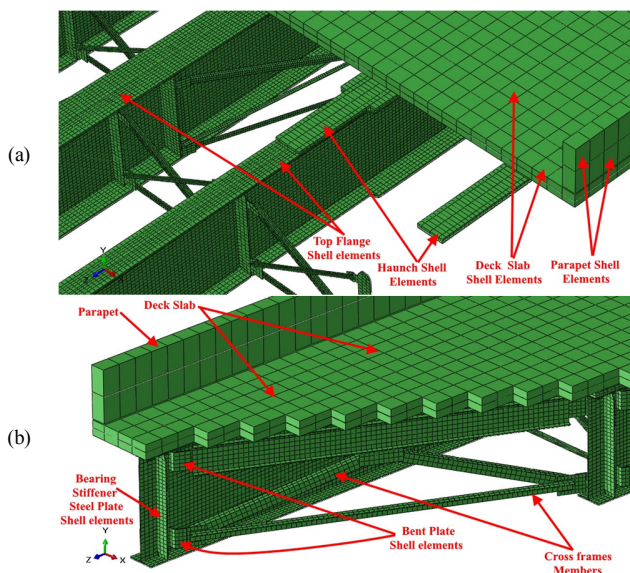


Fig. 6. Abaqus finite element model (static/shell model) for the US13 Bridge: (a) Pier support region, (b) abutment support region.

For modeling the concrete deck, haunch, and concrete guard wall, four-node reduced-integration shell elements (S4R) were used in the static models. For comparison, the dynamic models use three-dimensional eight-node reduced-integration brick elements (C3D8R) [16-18]. Reinforcement in the concrete is defined by Abaqus' rebar option using the actual geometry of the reinforcement and its spacing in both the static and dynamic models. In general, the mesh size of both the concrete deck slab and the metal forms was 30cm×30cm (1ft×1ft), while 8 or 12 elements were used across the width of the girder's top and bottom flanges and 28 elements through the height of each web. Linear isotropic elastic material properties were used for the FEA because the applied loads' result does not cause the proportional limit of the materials to

be exceeded. Expansion bearings, at abutments, were modeled with translation constraints in both vertical and transverse directions at the center node of the bottom flange cross-section of each girder, and only vertical direction constraint for the remaining bottom flange nodes of the abutment cross-sections. Fixed bearings, at the pier, were modeled similar to the expansion bearing constraints except that the center node of the bottom flange cross-sections was also restrained in the longitudinal direction.

B. Loading (Vehicle Modeling)

Two different approaches were used for modeling the static versus dynamic load passes. In the static models, the loading truck was modeled using six-point loads (one to represent each physical wheel of the loading vehicle). A Visual Basic for Applications (VBA) programming routine was used to model the variable nodal positions of the load as the truck traveled across the bridge for each load case. In this approach, only the load being transferred to the bridge due to the vehicle's weight is considered and the inertia of the vehicle is ignored. Previous studies classified moving load modeling (for the dynamic models) into three main types based on the technique used to model the vehicle. In one-dimensional (1D) models [19, 20] the vehicle is modeled as a spring-mass of one or two degrees of freedom, a planar model with multiple axles is considered in two-dimensional (2D) models [21, 22], and there are the 3D complete vehicle models [23, 24]. In this study, the one-dimensional (1D) dynamic model was adopted, where each wheel of the truck was modeled as a moving mass by defining a load versus time history for each axle, which is constant, and a displacement history for the position versus time. Consequently, both load and inertia are used to evaluate the dynamic effects of the moving load. Surface-based contact with a rigid pressure-overclosure relationship and frictionless tangential behavior was used to model the interaction between the bridge and moving masses.

C. Interaction Mechanisms and Analysis

Tie constraints were used to simulate all connections between the steel components of the bridge (e.g. between cross-frame members and vertical connection plates on the girders) for both the static and the dynamic models. The metal decking and the top flange were connected via merged nodes with all degrees of freedom constrained. Timoshenko (shear flexible) beam elements [16] with circular cross-sections and six degrees of freedom (three translational and three rotational) at each node to represent the shear studs and an isotropic friction model with a coefficient of friction of 0.4 at the steel-concrete interface were used to model the steel-concrete interaction mechanism in the dynamic models, while in the static ones, surface-to-surface tie constraints were used to model the connection between the haunch and the slab, and node-to-surface tie constraints were used to model the connection between the top flange and the haunch. The analysis was performed using an Expert Subroutine System programmed to extract key information from the Abaqus output result file [15]. This was implemented using the Caviness High-Performance Computing (HPC) cluster at the University of Delaware, USA. The static analysis was performed using Abaqus standard implicit static analysis while Abaqus explicit dynamic analysis was used for the dynamic models.

IV. FINITE ELEMENT VALIDATION

Figures 7 and 8 illustrate the maximum tensile and compressive stresses respectively, recorded from the field test and the FEA data for all girder strain gauges.

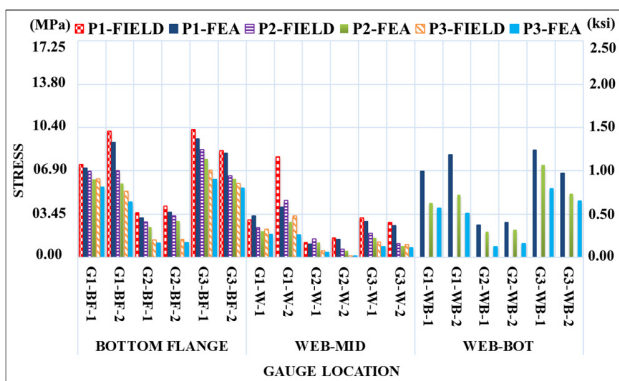


Fig. 7. Maximum tensile stress recorded from field test vs FEA data for all gauges located in the instrumented sections (G1, G2, and G3) due to the three passes.

Generally, the FEA accurately reproduces the general trends observed in the field testing and a favorable quantitative comparison is obtained in most cases, especially for the gauges located in the bottom flanges of the instrumented sections, and even more so when these gauges are in tension during Passes #1 and #2 (for Pass #1, there is 7.7% difference between the FEA and field test for tensile and 10.6% for compressive stresses, for Pass #2, 10.5% for tensile and 14.8% for compressive stresses, while for Pass #3, 13.4% for tensile and 18.9% for compressive stresses). A weaker correlation was

expected and achieved when comparing the compressive stress results since a linear elastic material with infinite tensile strength was used to model the concrete in tension. For the webs, the best overall correlation between these results was achieved during Pass #1 at the G2 gauge location during tension and compression, where the error is 8% or less. The overall average percentage errors are: for Pass #1, 12.43% for tension and 15.97% for compression, for Pass #2, 21.16% for tension and 23.49% for compression, and for Pass #3, 27.36% for tension and 31.28% for compression.

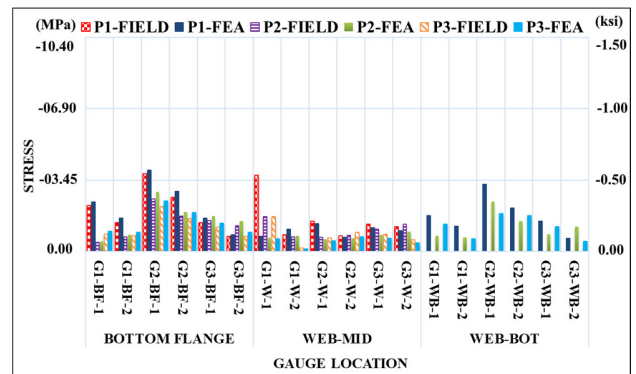


Fig. 8. Maximum compressive stress recorded from field test vs FEA data for all gauges located in the instrumented sections (G1, G2, and G3) due to the three passes.

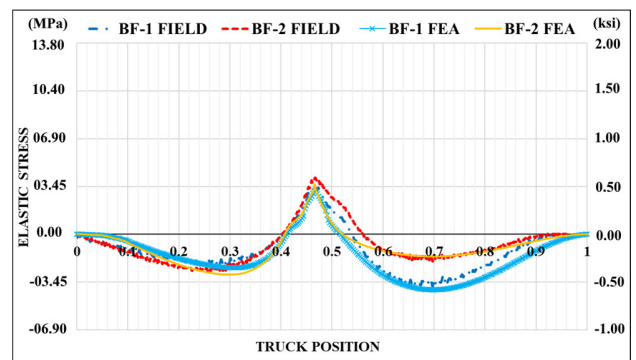


Fig. 9. Field vs FEA stresses influence line for the pair of gauges located in the bottom flange of the instrumented section G2.

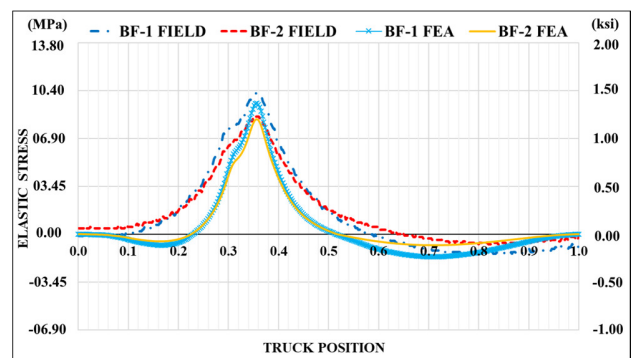


Fig. 10. Field vs FEA stresses influence line for the pair of gauges located in the bottom flange of the instrumented section G3.

Figures 9, 10 show the field results versus the FEA data for the bottom flange gauge positions G2 and G3 respectively in terms of stress versus truck position as it travels across the bridge. These Figures reveal that the FEA results match the expected trends in stress versus time as the truck travels across the bridge, including that the FEA also accurately captures the load locations that causing peak stress. It is worth mentioning that in Figures 9, 10, the x-axis represents the position of the truck as it travels over the two spans of the bridge. The value 0 of the x-axis declares that the truck is over the left support, the value 0.5 indicates that the truck reaches the intermediate support, while the value 1 shows that the truck is over the right support.

V. DYNAMIC LOAD FACTOR RESULTS

A. Dynamic Load Factors for G1, G2, and G3 Sections

Tables I and II illustrate the FEA maximum tensile and compressive stresses for different locations across the height of the cross-sections G1, G2, and G3 during the six Passes.

TABLE I. FEA MAXIMUM TENSILE STRESSES FOR INSTRUMENTED SECTIONS G1, G2, AND G3 DURING THE SIX PASSES

FEA MAXIMUM TENSILE STRESS							
PASSES	Gauge Location	SECTION G1		SECTION G2		SECTION G3	
		BF-1 MPa (ksi)	BF-2 MPa (ksi)	BF-1 MPa (ksi)	BF-2 MPa (ksi)	BF-1 MPa (ksi)	BF-2 MPa (ksi)
PASS#1	Bottom Flange	7.122	9.136	3.130	3.599	9.439	8.288
		(1.033)	(1.325)	(0.454)	(0.522)	(1.369)	(1.202)
		6.226	5.895	2.420	2.889	7.853	6.247
		(0.903)	(0.855)	(0.351)	(0.419)	(1.139)	(0.906)
		5.585	4.420	1.158	1.186	6.219	5.536
		(0.810)	(0.641)	(0.168)	(0.172)	(0.902)	(0.803)
PASS#2	Bottom Flange	9.485	11.935	3.772	4.546	10.251	9.470
		(1.376)	(1.731)	(0.547)	(0.659)	(1.487)	(1.373)
		8.103	7.487	2.859	3.607	8.436	7.067
		(1.175)	(1.086)	(0.415)	(0.523)	(1.224)	(1.025)
		7.111	5.565	1.359	1.464	6.627	6.229
		(1.031)	(0.807)	(0.197)	(0.212)	(0.961)	(0.903)
PASS#3	Bottom Flange	3.309	3.999	1.062	1.420	2.841	2.544
		(0.480)	(0.580)	(0.154)	(0.206)	(0.412)	(0.369)
		2.096	2.827	1.186	0.517	1.538	0.883
		(0.304)	(0.410)	(0.172)	(0.075)	(0.223)	(0.128)
		1.827	1.800	0.393	0.103	0.869	0.772
		(0.265)	(0.261)	(0.057)	(0.015)	(0.126)	(0.112)
PASS#4	Bottom Flange	3.718	4.819	1.172	1.639	3.000	2.740
		(0.539)	(0.699)	(0.170)	(0.238)	(0.435)	(0.397)
		2.326	3.347	1.283	0.585	1.613	0.935
		(0.337)	(0.485)	(0.186)	(0.085)	(0.234)	(0.136)
		1.994	2.099	0.423	0.116	0.899	0.815
		(0.289)	(0.304)	(0.061)	(0.017)	(0.130)	(0.118)
PASS#5	Bottom Flange	6.853	8.184	2.576	2.792	8.523	6.722
		(0.994)	(1.187)	(0.374)	(0.405)	(1.236)	(0.975)
		4.343	4.978	2.033	2.196	7.342	5.060
		(0.630)	(0.722)	(0.295)	(0.318)	(1.065)	(0.734)
		3.934	3.502	0.869	1.091	5.473	4.477
		(0.571)	(0.508)	(0.126)	(0.158)	(0.794)	(0.649)
PASS#6	Bottom Flange	8.722	9.972	3.050	3.257	9.131	7.628
		(1.265)	(1.446)	(0.442)	(0.472)	(1.324)	(1.106)
		5.393	5.985	2.374	2.716	7.773	5.638
		(0.782)	(0.868)	(0.344)	(0.394)	(1.127)	(0.818)
		4.848	4.166	1.012	1.342	5.746	4.961
		(0.703)	(0.604)	(0.147)	(0.195)	(0.833)	(0.720)
PASS#1	Web Mid	3.309	3.999	1.062	1.420	2.841	2.544
		(0.480)	(0.580)	(0.154)	(0.206)	(0.412)	(0.369)
		2.096	2.827	1.186	0.517	1.538	0.883
		(0.304)	(0.410)	(0.172)	(0.075)	(0.223)	(0.128)
		1.827	1.800	0.393	0.103	0.869	0.772
		(0.265)	(0.261)	(0.057)	(0.015)	(0.126)	(0.112)
PASS#2	Web Mid	3.718	4.819	1.172	1.639	3.000	2.740
		(0.539)	(0.699)	(0.170)	(0.238)	(0.435)	(0.397)
		2.326	3.347	1.283	0.585	1.613	0.935
		(0.337)	(0.485)	(0.186)	(0.085)	(0.234)	(0.136)
		1.994	2.099	0.423	0.116	0.899	0.815
		(0.289)	(0.304)	(0.061)	(0.017)	(0.130)	(0.118)
PASS#3	Web Mid	6.853	8.184	2.576	2.792	8.523	6.722
		(0.994)	(1.187)	(0.374)	(0.405)	(1.236)	(0.975)
		4.343	4.978	2.033	2.196	7.342	5.060
		(0.630)	(0.722)	(0.295)	(0.318)	(1.065)	(0.734)
		3.934	3.502	0.869	1.091	5.473	4.477
		(0.571)	(0.508)	(0.126)	(0.158)	(0.794)	(0.649)
PASS#4	Web Mid	8.722	9.972	3.050	3.257	9.131	7.628
		(1.265)	(1.446)	(0.442)	(0.472)	(1.324)	(1.106)
		5.393	5.985	2.374	2.716	7.773	5.638
		(0.782)	(0.868)	(0.344)	(0.394)	(1.127)	(0.818)
		4.848	4.166	1.012	1.342	5.746	4.961
		(0.703)	(0.604)	(0.147)	(0.195)	(0.833)	(0.720)
PASS#5	Web Mid	3.309	3.999	1.062	1.420	2.841	2.544
		(0.480)	(0.580)	(0.154)	(0.206)	(0.412)	(0.369)
		2.096	2.827	1.186	0.517	1.538	0.883
		(0.304)	(0.410)	(0.172)	(0.075)	(0.223)	(0.128)
		1.827	1.800	0.393	0.103	0.869	0.772
		(0.265)	(0.261)	(0.057)	(0.015)	(0.126)	(0.112)
PASS#6	Web Mid	3.718	4.819	1.172	1.639	3.000	2.740
		(0.539)	(0.699)	(0.170)	(0.238)	(0.435)	(0.397)
		2.326	3.347	1.283	0.585	1.613	0.935
		(0.337)	(0.485)	(0.186)	(0.085)	(0.234)	(0.136)
		1.994	2.099	0.423	0.116	0.899	0.815
		(0.289)	(0.304)	(0.061)	(0.017)	(0.130)	(0.118)
PASS#1	Web Bot	6.853	8.184	2.576	2.792	8.523	6.722
		(0.994)	(1.187)	(0.374)	(0.405)	(1.236)	(0.975)
		4.343	4.978	2.033	2.196	7.342	5.060
		(0.630)	(0.722)	(0.295)	(0.318)	(1.065)	(0.734)
		3.934	3.502	0.869	1.091	5.473	4.477
		(0.571)	(0.508)	(0.126)	(0.158)	(0.794)	(0.649)
PASS#2	Web Bot	8.722	9.972	3.050	3.257	9.131	7.628
		(1.265)	(1.446)	(0.442)	(0.472)	(1.324)	(1.106)
		5.393	5.985	2.374	2.716	7.773	5.638
		(0.782)	(0.868)	(0.344)	(0.394)	(1.127)	(0.818)
		4.848	4.166	1.012	1.342	5.746	4.961
		(0.703)	(0.604)	(0.147)	(0.195)	(0.833)	(0.720)

Figures 11 and 12 illustrate the DLF results for all gauges installed on G1, G2, and G3 sections, (see Figure 4), due to the static and dynamic passes shown in Figure 5 in terms of maximum tensile and compressive stresses respectively. The goal of this preliminary analysis is to evaluate the passes that produced higher DLF values.

TABLE II. FEA MAXIMUM COMPRESSIVE STRESSES FOR INSTRUMENTED SECTIONS G1, G2, AND G3 DURING THE SIX PASSES

FEA MAXIMUM COMPRESSIVE STRESS							
PASSES	Gauge Location	SECTION G1		SECTION G2		SECTION G3	
		BF-1 MPa (ksi)	BF-2 MPa (ksi)	BF-1 MPa (ksi)	BF-2 MPa (ksi)	BF-1 MPa (ksi)	BF-2 MPa (ksi)
PASS#1	Bottom Flange	-2.386	-1.613	-3.937	-2.903	-1.613	-0.793
		(-0.346)	(-0.234)	(-0.571)	(-0.421)	(-0.234)	(-0.115)
		-0.496	-0.793	-2.882	-1.910	-1.710	-1.462
		(-0.072)	(-0.115)	(-0.418)	(-0.277)	(-0.248)	(-0.212)
		-0.972	-0.931	-2.434	-1.882	-1.358	-0.924
		(-0.141)	(-0.135)	(-0.353)	(-0.273)	(-0.197)	(-0.134)
PASS#2	Bottom Flange	-3.216	-2.207	-4.696	-3.653	-1.797	-0.911
		(-0.466)	(-0.320)	(-0.681)	(-0.530)	(-0.261)	(-0.132)
		-0.656	-1.065	-3.374	-2.379	-1.870	-1.645
		(-0.095)	(-0.155)	(-0.489)	(-0.345)	(-0.271)	(-0.239)
		-1.278	-1.243	-2.795	-2.300	-1.461	-1.028
		(-0.185)	(-0.180)	(-0.405)	(-0.334)	(-0.212)	(-0.149)
PASS#3	Bottom Flange	3.309	-1.069	-1.351	-0.683	-1.145	-1.007
		(-0.106)	(-0.155)	(-0.196)	(-0.099)	(-0.166)	(-0.146)
		-0.662	-0.752	-0.572	-0.627	-0.814	-0.958
		(-0.096)	(-0.109)	(-0.083)	(-0.091)	(-0.118)	(-0.139)
		-0.614	-0.131	-0.510	-0.696	-0.641	-0.407
		(-0.089)	(-0.019)	(-0.074)	(-0.101)	(-0.093)	(-0.059)
PASS#4	Bottom Flange	-0.857	-1.314	-1.535	-0.813	-1.207	-1.134
		(-0.124)	(-0.191)	(-0.223)	(-0.118)	(-0.175)	(-0.165)
		-0.771	-0.917	-0.642	-0.742	-0.851	-1.076
		(-0.112)	(-0.133)	(-0.093)	(-0.108)	(-0.123)	(-0.156)
		-0.702	-0.157	-0.562	-0.816	-0.665	-0.455
		(-0.102)	(-0.023)	(-0.081)	(-0.118)	(-0.096)	(-0.066)
PASS#5	Bottom Flange	6.853	-1.210	-3.240	-2.090	-1.457	-0.643
		(-0.251)	(-0.176)	(-0.470)	(-0.303)	(-0.211)	(-0.093)
		-0.766	-0.670	-2.421	-1.451	-0.816	-1.184
		(-0.111)	(-0.097)	(-0.351)	(-0.211)	(-0.118)	(-0.172)
		-1.311	-0.618	-1.825	-1.732	-1.195	-0.497
		(-0.190)	(-0.090)	(-0.265)	(-0.251)	(-0.173)	(-0.072)
PASS#6	Bottom Flange	-2.235	-1.594	-3.845	-2.531	-1.507	-0.727
		(-0.324)	(-0.231)	(-0.558)	(-0.367)	(-0.219)	(-0.105)
		-0.968	-0.871	-2.807	-1.726	-0.820	-1.305
		(-0.140)	(-0.126)	(-0.407)	(-0.250)	(-0.119)	(-0.189)
		-1.637	-0.791	-2.090	-2.006	-1.166	-0.540
		(-0.237)	(-0.115)	(-0.303)	(-0.291)	(-0.169)	(-0.078)

In general, both Figures 11 and 12 revealed that the ratio between Pass#4 (dynamic) and Pass#1 (static), generates the higher dynamic responses compared to the other passes in terms of DLF. This suggests that the ideal use of the model is when the load is placed as close to the girder of interest as possible (instrumented section), which also has the benefit of producing the highest stresses in the member of interest. The average DLF value for the spots investigated in the web's middle region is 1.10, while 1.17 and 1.21 are the DLFs for the web's bottom region and the spots at the bottom flange cross-section respectively. In Figures 11-12, the data series titled "AASHTO LRFD" refer to the value of 1.33 (DLA=0.33 ⇒ DLF=1+DLA=1.33), used by AASHTO LRFD specifications.

DLF of 1.25 and 1.4 was used for the data series "BS5400" and "OHBD" respectively. The series titled "AASHTO (US13)" refers to the output of (3) using US13 Bridge span Length.

B. Dynamic Load Factors for Girder Cross-Sections Adjacent to Cross-Frames Located at Girder#4

The preliminary investigation revealed that Passes #1 and #4 result in higher values of DLF especially for the gauges located at the bottom flange section of the instrumented girder (Girder #4).

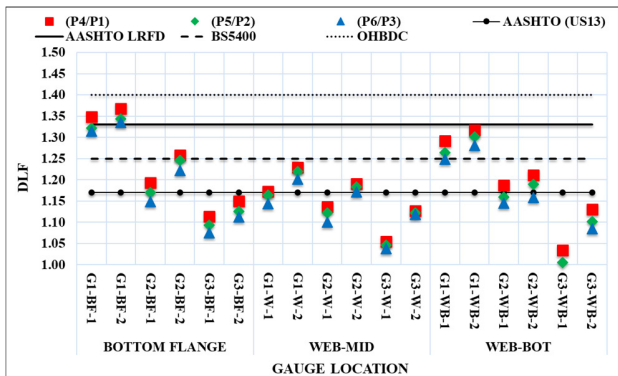


Fig. 11. FEA dynamic load factor values for instrumented sections G1, G2, and G3 in terms of tensile stresses.

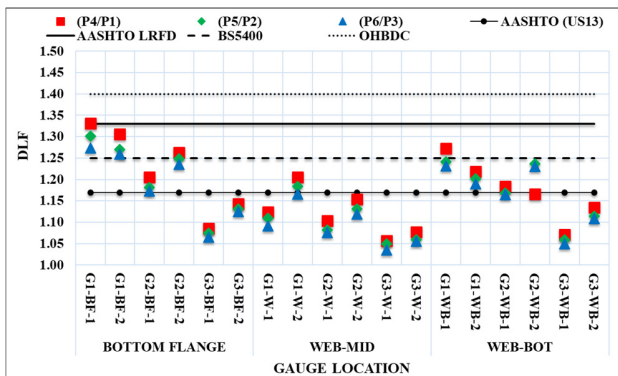


Fig. 12. FEA dynamic load factor values for instrumented sections G1, G2, and G3 in terms of compressive stresses.

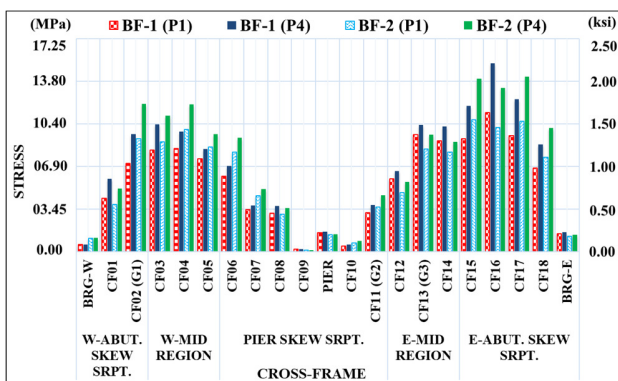


Fig. 13. FEA maximum tensile stresses for BF-1 and BF-2 locations at girder cross-sections adjacent to cross-frames connected to Girder #4 due to truck Pass#1 and Pass#4.

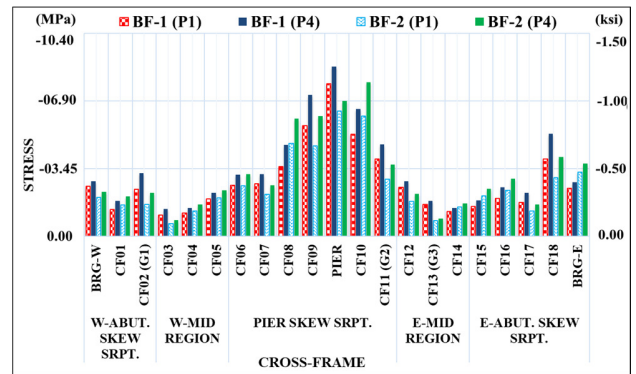


Fig. 14. FEA maximum compressive stresses for BF-1 and BF-2 locations at girder cross-sections adjacent to cross-frames connected to Girder #4 due to truck Pass#1 and Pass#4.

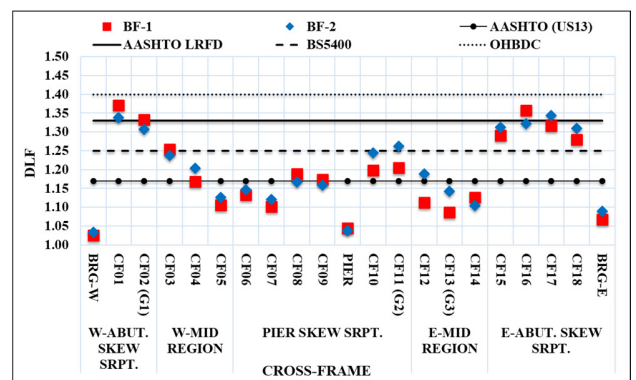


Fig. 15. FEA dynamic load factor variation along the bottom flange of Girder #4 in terms of maximum tensile stresses.

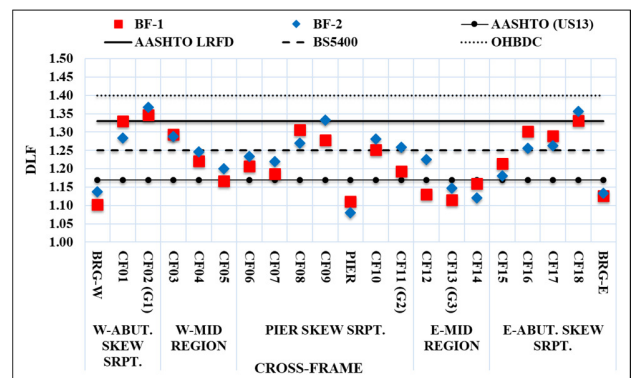


Fig. 16. FEA dynamic load factor variation along the bottom flange of Girder #4 in terms of maximum compressive stresses.

In Figures 13-16, the symbols BRG-W, and BRG-E refer to the west and east bridge expansion bearing supports, and PIER, refer to the pier fixed bearing support, while CF#, refer to the cross-frame adjacent to the girder#4 cross-section (see Figure 3). Figures 15 and 16 show the DLF variation along the bottom flange of Girder #4. The higher DLF values are concentrated near the skew support regions (abutments). This is hypothesized as being due to the skew bridge support regions, which are subjected to significant torsional and lateral moments due to the interaction effect of both the bracing system and the moving loads. It is hypothesized that the dynamic responses of

the bridge exacerbate these effects. The average DLF values for the abutments skew support regions are 1.25 in tension and 1.27 in compression, and for the pier skew support region 1.16 in tension and 1.22 in compression, while for the non-skew middle region they are 1.15 in tension and 1.18 in compression.

VI. CASE STUDY

This case study is implemented in order to investigate the effect of different arrangements of bracing systems on the

bridge dynamic response and thus on DLF values. Figure 17 represents the US13 Bridge but with staggered cross-frames configuration keeping the other components of the bridge the same as in the real bridge. Sections G1, G2, and G3 in addition to cross-frames CF1, CF8, CF15, CF16, and CF17 are selected to compare the DLF results for perpendicular vs staggered cross-frames configuration of the US13 Bridge. These sections (bottom flange sections) are selected since they are matching in locations in perpendicular and staggered bracing systems of US13 Bridge as shown in Figures 5 and 17 respectively.

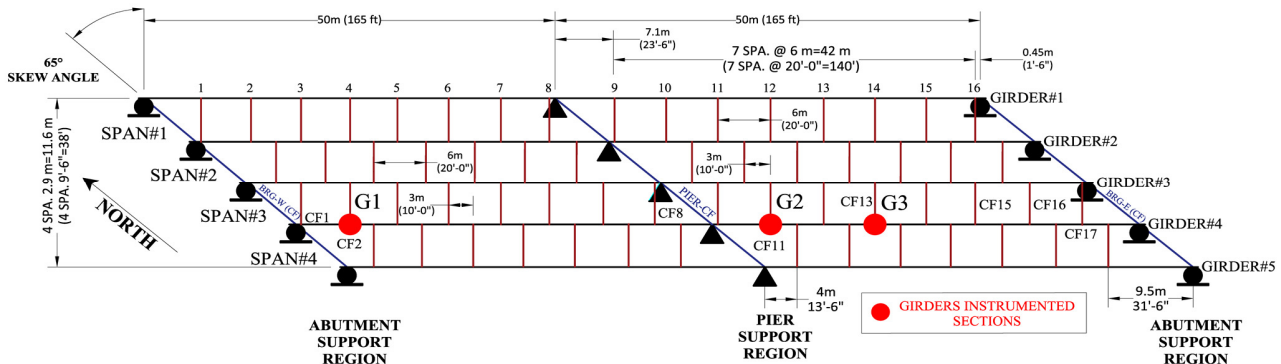


Fig. 17. US13 Bridge with staggered cross-frames configuration.

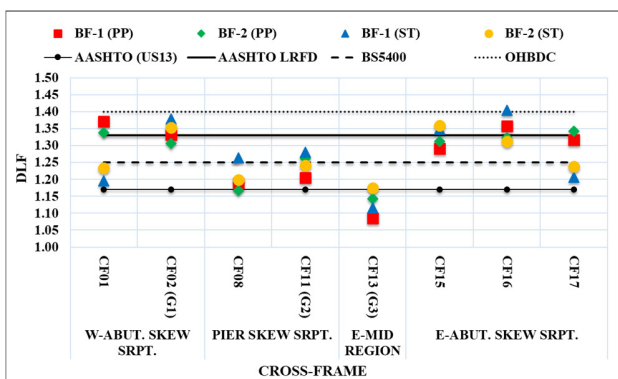


Fig. 18. FEA perpendicular vs staggered DLFs for selected sections along the bottom flange of Girder #4 in terms of maximum tensile stresses.

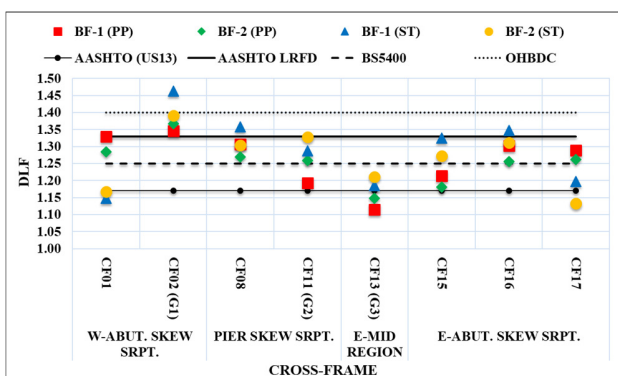


Fig. 19. FEA perpendicular vs staggered DLFs for selected sections along the bottom flange of Girder #4 in terms of maximum compressive stresses.

Figures 18 and 19 show the comparison of the DLF results for both cases. The comparisons indicate a slight difference between the DLFs results of both perpendicular and staggered cross-frames configurations within this range of bridge length and skew angle. For the selected cross-frames, the average DLF values in tensions are 1.25 for perpendicular bracing and 1.26 for staggered bracing, while in compression the average values are 1.26 and 1.28 for perpendicular and staggered bracing respectively.

VII. CONCLUSION

Field testing data of different passes of a weighed load vehicle were used to validate a full-scale 3D FEA model of a highly skewed steel girder bridge, created with the FEA software ABAQUS/CAE. The results include the maximum tension and compression stresses resulting from static and dynamic travel speeds along the length of the most-heavily loaded girder. These are used to calculate DLF and are compared with the code provisions for DLF. The results of this study lead to the following conclusions:

- The DLF is highly variable throughout the length of the girder and the results indicate that the DLF from the compressive stresses of the skewed continuous bridge is larger than those for tensile stresses. The average value for all cross-frames DLF in tension is 1.19 and in compression is 1.23.
- The DLF used in the current practice codes is intended for the design of new bridges and the case of in-service bridges. This shows that most codes of practice are appropriately conservative in the regions of the girder that would govern the flexural design. However, the DLF sometimes exceeds the code-recommended values in the

vicinity of skewed supports. The discrepancy of the DLF, in the west abutment skew support region, exceeds by 13% and 16% the values determined by [2] for tension and compression stresses respectively, while in comparison to [8] the differences reach 6% and 8%, respectively.

According to the review of the widely used codes of practice, it can be concluded that the specifications related to DLF vary significantly, indicating that there is no unanimity for the evaluation of DLF. Also, only a few parameters are adopted in the expression of DLF, such as bridge span length in [2-4], bridge natural frequency [5, 6], and traffic load models in [7, 8]. The outputs of this study were based on the numerical models on a skew continuous girder bridge with specific span length and skew. More diverse numerical investigations or field testing of bridges with a wider range of both span lengths and skewness are suggested to draw a more comprehensive perspective on the general dynamic behavior of the skewed continuous and simple span bridges. Also, more studies are needed in order to evaluate the effect of skewness and bracing system configurations (e.g. perpendicular, parallel, and staggered) on the bridge dynamic responses.

REFERENCES

- [1] H. Moghimi and H. Ronagh, "Impact factors for a composite steel bridge using non-linear dynamic simulation," *International Journal of Impact Engineering*, vol. 35, no. 11, pp. 1228–1243, Nov. 2008, <https://doi.org/10.1016/j.ijimpeng.2007.07.003>.
- [2] *Standard Specifications for Highway Bridges: 2002*, 17th edition. Washington, DC, USA: AASHTO, 2003.
- [3] *Specifications for highway bridges. Part 1: Common Specifications*. Tokyo, Japan: Japan Road Association, 1996.
- [4] *Load and Resistance Factor Design Specifications*, 8th ed. Washington DC, USA: AASHTO, 2017.
- [5] *Ontario Highway Bridge Design Code*, 2nd ed. Toronto, Canada: Ontario Ministry of Transportation and Communications, 1983.
- [6] *Bridge Design Code*. Sydney, Australia: Australia's National Road Authority, 1992.
- [7] *Eurocode 1: Actions on structures - Part 2: Traffic loads on bridges*. Brussels, Belgium: CEN, 2003.
- [8] *BSS400-2: Steel, Concrete and Composite Bridges. Part 2: Specification for Loads*. London, UK: BSI, 2006.
- [9] L. Ma, W. Zhang, W. S. Han, and J. X. Liu, "Determining the dynamic amplification factor of multi-span continuous box girder bridges in highways using vehicle-bridge interaction analyses," *Engineering Structures*, vol. 181, pp. 47–59, Feb. 2019, <https://doi.org/10.1016/j.engstruct.2018.11.059>.
- [10] W. Wang, L. Deng, and X. Shao, "Fatigue Design of Steel Bridges Considering the Effect of Dynamic Vehicle Loading and Overloaded Trucks," *Journal of Bridge Engineering*, vol. 21, no. 9, Sep. 2016, Art. no. 04016048, [https://doi.org/10.1061/\(ASCE\)BE.1943-5592.0000914](https://doi.org/10.1061/(ASCE)BE.1943-5592.0000914).
- [11] X. Zhang, K. Sennah, and J. B. Kennedy, "Evaluation of impact factors for composite concrete-steel cellular straight bridges," *Engineering Structures*, vol. 25, no. 3, pp. 313–321, Feb. 2003, [https://doi.org/10.1016/S0141-0296\(02\)00160-8](https://doi.org/10.1016/S0141-0296(02)00160-8).
- [12] Y.-B. Yang, S.-S. Liao, and B.-H. Lin, "Impact Formulas for Vehicles Moving over Simple and Continuous Beams," *Journal of Structural Engineering*, vol. 121, no. 11, pp. 1644–1650, Nov. 1995, [https://doi.org/10.1061/\(ASCE\)0733-9445\(1995\)121:11\(1644\)](https://doi.org/10.1061/(ASCE)0733-9445(1995)121:11(1644)).
- [13] "BDI strain transducer ST-350 specifications sheet." BDI, 2006.
- [14] J. R. McConnell, M. Radovic, and K. Ambrose, "Field Evaluation of Cross-Frame and Girder Live-Load Response in Skewed Steel I-Girder Bridges," *Journal of Bridge Engineering*, vol. 21, no. 3, Mar. 2016, Art. no. 04015062, [https://doi.org/10.1061/\(ASCE\)BE.1943-5592.0000846](https://doi.org/10.1061/(ASCE)BE.1943-5592.0000846).
- [15] Y. Almoosi, J. McConnell, and N. Oukaili, "Structural Modeling of Cross-Frame Behavior in Steel Girder Bridges," in *2019 12th International Conference on Developments in eSystems Engineering (DeSE)*, Kazan, Russia, Oct. 2019, pp. 620–625, <https://doi.org/10.1109/DeSE.2019.00117>.
- [16] *ABAQUS 6.14: ABAQUS/CAE user's guide*. Simulia, 2019.
- [17] M. a. J. Hassan and A. F. Izzet, "Experimental and Numerical Comparison of Reinforced Concrete Gable Roof Beams with Openings of Different Configurations," *Engineering, Technology & Applied Science Research*, vol. 9, no. 6, pp. 5066–5073, Dec. 2019, <https://doi.org/10.48084/etasr.3188>.
- [18] H. M. Hekmet and A. F. Izzet, "Numerical Analysis of Segmental Post Tensioned Concrete Beams Exposed to High Fire Temperature," *Engineering, Technology & Applied Science Research*, vol. 9, no. 5, pp. 4759–4768, Oct. 2019, <https://doi.org/10.48084/etasr.3059>.
- [19] D. Chang and H.-H. Lee, "Impact Factors for Simple-Span Highway Girder Bridges," *Journal of Structural Engineering*, vol. 120, no. 3, pp. 704–715, Mar. 1994, [https://doi.org/10.1061/\(ASCE\)0733-9445\(1994\)120:3\(704\)](https://doi.org/10.1061/(ASCE)0733-9445(1994)120:3(704)).
- [20] Y.-B. Yang, C. W. Lin, and J. D. Yau, "Extracting bridge frequencies from the dynamic response of a passing vehicle," *Journal of Sound and Vibration*, vol. 272, no. 3, pp. 471–493, May 2004, [https://doi.org/10.1016/S0022-460X\(03\)00378-X](https://doi.org/10.1016/S0022-460X(03)00378-X).
- [21] P. K. Chatterjee, T. K. Datta, and C. S. Surana, "Vibration of Suspension Bridges under Vehicular Movement," *Journal of Structural Engineering*, vol. 120, no. 3, pp. 681–703, Mar. 1994, [https://doi.org/10.1061/\(ASCE\)0733-9445\(1994\)120:3\(681\)](https://doi.org/10.1061/(ASCE)0733-9445(1994)120:3(681)).
- [22] K. Chompooming and M. Yener, "The influence of roadway surface irregularities and vehicle deceleration on bridge dynamics using the method of lines," *Journal of Sound and Vibration*, vol. 183, no. 4, pp. 567–589, Jun. 1995, <https://doi.org/10.1006/jsvi.1995.0273>.
- [23] D. Huang, T.-L. Wang, and M. Shahawy, "Impact Analysis of Continuous Multigirder Bridges due to Moving Vehicles," *Journal of Structural Engineering*, vol. 118, no. 12, pp. 3427–3443, Dec. 1992, [https://doi.org/10.1061/\(ASCE\)0733-9445\(1992\)118:12\(3427\)](https://doi.org/10.1061/(ASCE)0733-9445(1992)118:12(3427)).
- [24] E. J. OBrien, D. Cantero, B. Enright, and A. González, "Characteristic Dynamic Increment for extreme traffic loading events on short and medium span highway bridges," *Engineering Structures*, vol. 32, no. 12, pp. 3827–3835, Dec. 2010, <https://doi.org/10.1016/j.engstruct.2010.08.018>.